Journal of Advanced Multidisciplinary Research Studies and Development

ISSN : 2583-6404
Nov - Dec 2023

ANALYSIS ON THE SMALL PUNCH CREEP AND MODELLING OF CREEP DAMAGE

Sandeep Kumar[1], Dr. Milind Rohokale[2]

[1] *Research Scholar, Department of Mechanical Engineering, Himalayan University, Itanagar, A. P.*

[2] *Research Supervisor, Department of Mechanical Engineering, Himalayan University, Itanagar, A. P.*

Abstract

Introduction: The rotary friction welding process, also known as continuous drive friction welding, is a green welding technique used to join ferrous and non-ferrous materials of the same and different shapes and sizes.

Aim of the Study: The main aim of the study is Analysis on the Small Punch Creep and Modelling of Creep Damage

Material and Method: To reduce the remaining tensions created during the welding process, post-weld heat treatment (PWHT) was used.

Conclusion: Regarding the size and distribution of M23C6 precipitates, there were the most significant microstructural changes.

Keywords: Creep Damage, Modelling.

► *Corresponding Author: Sandeep Kumar*

1. Introduction

1.1 Rotary Friction Welding

The rotary friction welding process, also known as continuous drive friction welding, is a green welding technique used to join ferrous and non-ferrous materials of the same and different shapes and sizes. In addition, the friction welding procedure was the first of its kind, successfully joining a wide variety of materials with little effort. Because there is no melting point in friction welding, all the issues that arise during fusion welding are eliminated. On the other hand, the joint qualities are affected by the process parameters related to friction welding. Therefore, a sound joint cannot be achieved without careful selection of friction welding conditions.

The step involved in the friction welding process is comparatively easy and fabricating the joint is also much quicker than any other welding process. Two chucks are placed in the friction machine in which one is rotatable connected to the motor driven unit where as another one is located exactly opposite to rotating chuck and connected by means of lead screw to achieve the transverse motion. Hence, the work pieces are attached in the respective chuck to accomplish the rotary and transverse motions. The motor unit present in the welding process is a specially designed synchronized motor so that it can be stopped abruptly by preset time. Moreover the friction welding process contains four important steps such as rotation of one side work piece, axial movement of opposite work piece, friction between the rubbing faces and forging process by upset or axial load to consolidate the material to confirm the weld. During the process, the rubbing actions between the two faces of the work piece turn into generating the frictional heat which attains the metal deformation. Due to this the detachment material from both side, the plastically deformed material mixed with each other and consolidated at the weld interface to confirm the joint when the forging action take place.

ISSN : 2583-6404
Nov - Dec 2023

The forging actions lead to the deformed materials in radial flow towards outside from the weld interface. This outward flow of materials is to develop the flashes at the outer circumference weld joint. To attain the proper forging actions the upset load and upset time are encoded based on the requirement. The schematic diagram represents the stages of friction welding process are shown in figure 1.1.

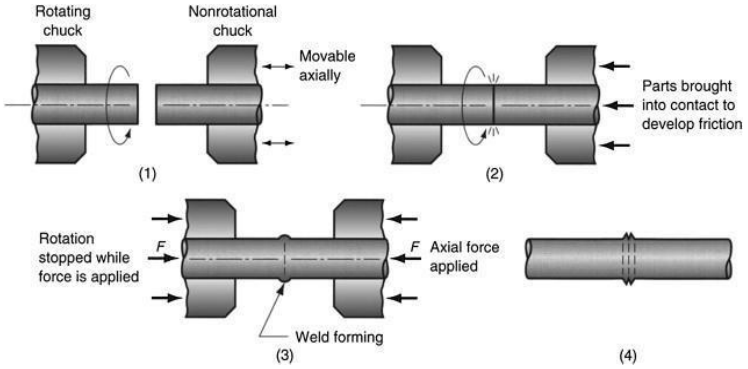

Figure 1.1 Stages of rotary friction welding process

2. Literature Review

Sakthivel *et al.* (2020) studied the microstructures and impression creep characteristics of the P91 steel joints fabricated by the ATIG welding process. The weld joints are subjected to PWHT (1033/1hr) then the ICT samples are prepared with the dimensions of 20 x 10 x 10 mm^3. Impression creep behavior was studied in the HAZ and weld metal regions at the temperature of 923 K with different stress levels (180 MPa, 240 MPa, 300 MPa, and 330 MPa). It is found that the ICHAZ exhibited higher deformation, CGHAZ experienced significantly less deformation. ICHAZ was depicted with less lath morphology, this had an impact on faster deformation. Moreover, the presence of recovered and deformed structures with coarser M23C6 precipitates and less coincidence site lattice boundaries has induced high creep deformation as compared to the weld zone and HAZ.

XiaohuHao (2019) The titanium rich layer was formed in titanium inter metal compound and the depleted layer was observed in between of welded zone and titanium rich layer. The depleted zone were mainly presence of Ti ,Cr, and Fe phases. The FCC ductile phases were noted in welded zone. The Ti-Cu transition phased has revolved limited fracture zone during evaluation with higher micro hardness.

Shuhan Li (2019) reported that the effect of titanium and steel dissimilar butt joint by friction stir process. This dissimilar joint was achieved defect free welded specimen in 600 to 950 rpm rotating speed and 47.5 mm / min travel speed. When increased speed of rotation has executed significant grain size changes and thickest TiFe layer formation which was influenced to affecting joint hardness value. The TiFe layer formation on inter metallic compound layer was observed in EBSD analysis. That layer has ensured the strength of welded zone. The dissimilar joint could be achieved sufficient improved physical properties.

MuralimohanCheepu (2019) done research on titanium and stainless steel dissimilar material integrated with friction stir welding. The Ni inter layer was used in dissimilar joint process. It was formed significant TiNi phases in intermetallic zone. The Ni interlayer was controlled presence of dangerous brittle phases like Ti – Fe and Ti – Cr phases. It was used to achieve better joining efficiency. The welded zones and noted as limited micro crack and smooth morphology.

ISSN : 2583-6404
Nov - Dec 2023

Scherillo (2019) applied linear friction electron beam weld on Ti–6Al–4V. The collaboration of linear friction welding and electron beam welding was clearly investigated. The process was shown the best result leading wide range conditions. The base material original microstructure was not much more changes and also no evidence observed in heat affected zone. So he decided to conduct future investigation process for fatigue and tensile properties examination.

3. Methodology

3.1 Post Weld Heat Treatment

To reduce the remaining tensions created during the welding process, post-weld heat treatment (PWHT) was used. PWHT at 750–770 °C for 1–3 hours is advised because the tempering action at this temperature results in excellent toughness qualities and stable microstructures. In this investigation, PWHT of the weld joint was completed using a muffle furnace at 760 °C for 1 hour, followed by air cooling. As-welded specimens were initially removed from the weld plate for basic microstructural investigations, then PWHT.

4. Results

4.1 Small Punch Creep and Modelling of Creep Damage

under earlier sections, the structure-property connection was established utilising conventional tensile testing at room temperature as well as ABI testing for dissimilar weld joints under as welded and PWHT circumstances. The findings of this testing are also covered in full here.

4.1.1 Small punch creep

The heat affected zones (HAZ) of coarse grain (CG-HAZ), fine grain (FG-HAZ), and intercritical grain (IC-HAZ) of P91 steel base metal samples were studied. At a temperature of 600 °C (the actual service temperature), SPC tests were conducted with an applied force of 400 and 500 N maintained throughout the test. The SPC test was carried out until the punch had penetrated the material 2.5 mm. The outcomes are further addressed.

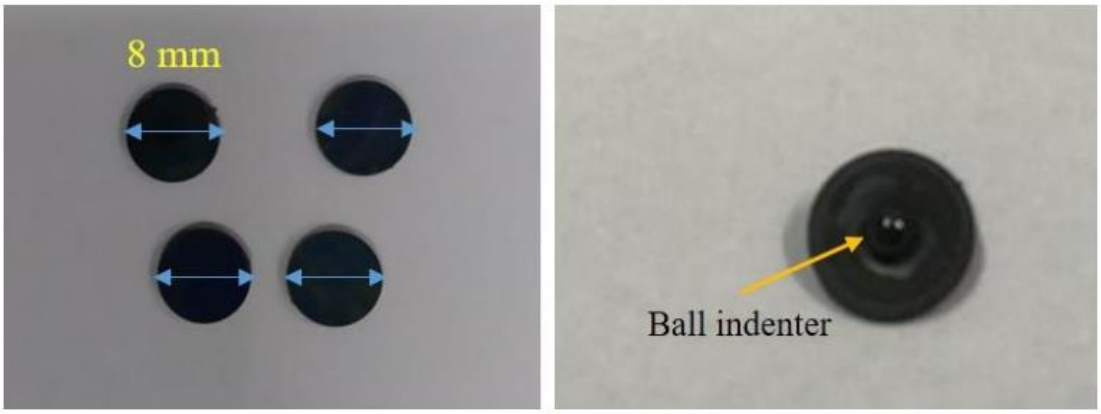

Fig. 4.1 SPC test specimens

4.1.1.1 SPC test results

Each HAZ area of P91 steel, including the CG-HAZ, FG-HAZ, ICHAZ, and base metal, was subjected to SPC testing as a single component region. Punch displacement and load data points

ISSN : 2583-6404
Nov - Dec 2023

with creep exposure time were collected in the SPC test until the depth of penetration reached 2.5 mm. The SPC life of a specimen was defined as the length of time it was exposed to high temperatures until the necessary depth of punch penetration was achieved. SPC curves (displacement vs. time) were produced and are shown in Fig. 4.2 (a) and (b) for uniaxial constant loads of 500 and 400 N, respectively. These curves are similar to the traditional creep curve (strain vs. time). The SPC curves, which display three stages—primary, secondary, and tertiary—exactly matched the traditional creep curves. However, a noticeable early bending deformation brought on by striking the test material resulted in a significant difference being shown at the first stage of the SPC curve.

SPC life was found to be maximum for P91 base metal (17.5 h) and lowest for IC-HAZ (6.5 h) under an applied load of 500 N. The SPC life in the CG-HAZ and FG-HAZ zones was around 12 hours. The SPC life of each component section of the P91 steel side increased when the applied load was reduced from 500 to 400 N. Similar SPC life trends were observed for applied loads of 400 N, with P91 base metal recording the highest SPC life of 80 h and IC-HAZ recording the lowest rupture life of 25 h. It may be deduced from the SPC data for both 500 and 400 N that IC-HAZ was the weakest ingredient overall. SPC curves revealed that the secondary stage for the IC-HAZ was much shorter than those for other locations at a certain applied stress. As a result, the IC-HAZ began the tertiary stage at the earliest possible time.

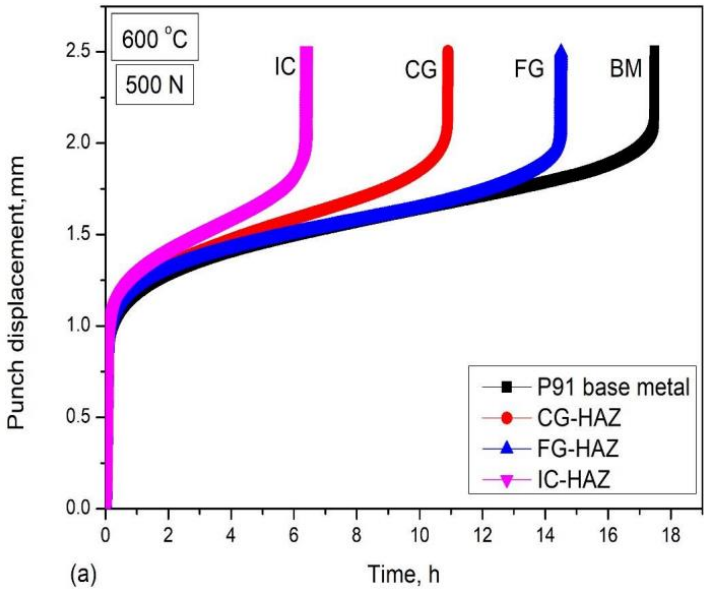

ISSN : 2583-6404
Nov - Dec 2023

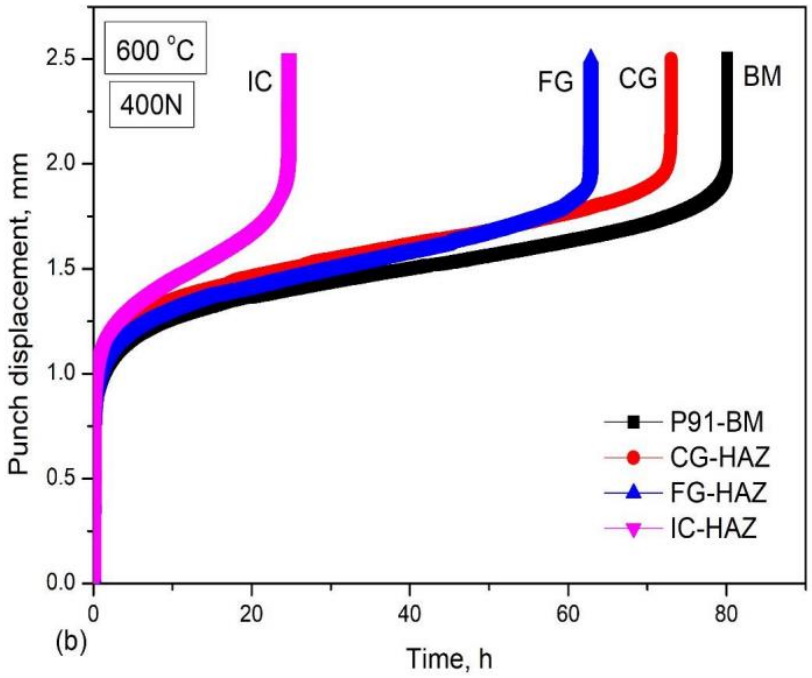

Fig. 4.2 Punch displacement vs. time (a) 500 N (b) 400 N

4.1.1.2 SPC results analysis

The minimal creep rate value for each location of the P91 HAZ and base metal was determined using SPC data and is shown in Table 4.1. Through this research, such values for specific HAZ zones have been published for the first time.

Table 4.1 SPC-Minimum creep rate at test temperature of 600 ℃

Load	**P91 Base Metal**	**CG-HAZ**	**FG-HAZ**	**IC-HAZ**
	(mm/h)	**(mm/h)**	**(mm/h)**	**(mm/h)**
500 N	0.02293	0.0416	0.02609	0.07419
400 N	0.00193	0.00285	0.00266	0.00914

The graph produced from the minimal creep rate vs. load data is given in Fig. 4.3. The IC-HAZ had the greatest minimum creep rate values with an applied load of 500 N (0.07419), while the base metal had the lowest values (0.02293). The 400 N applied load showed the same pattern. It has been documented in the literature that the relationship between the minimal creep rate and the applied force of an SPC test was defined by a power law similar to Norton's law (4.2) in the uniaxial creep scenario.

$$\dot{\varepsilon}_s = A\sigma^n$$

Following evaluations for each HAZ and base metal area, the constants A and n in the Norton law equation are shown in Table 4.5. The stress exponent value, n, was in the 9–12 range for all of the component sections, suggesting a consistent creep deformation process. The dissimilar weld joint's overall failure mechanism was controlled by this component, according to the greatest value of creep coefficient, A, determined for IC-HAZ. The FE study of the P91 HAZ and base metal, which is discussed in the next section, benefited from these constants for the various component areas.

ISSN : 2583-6404
Nov - Dec 2023

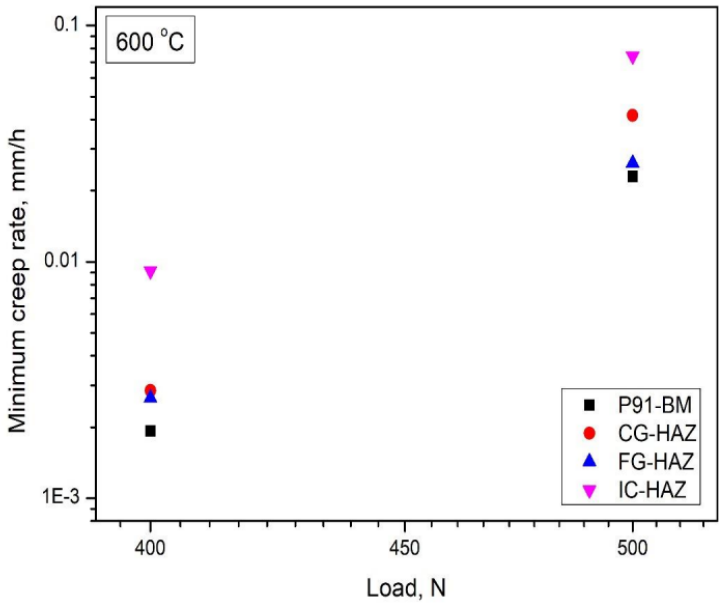

Fig. 4.3 Minimum creep rate vs. load

Table 4.2 Material constants for P91 steel HAZ and base metal

	A x 10^{-15} (MPa^{-n}/h)	**n**
CG-HAZ	2.9	12.01
FG-HAZ	208	10.7
IC-HAZ	3230	9.3
Base Metal	19.4	11.1

4.1.2 Finite element analysis

The programme ABAQUS 6.13 was used to do the finite element analysis. First, as illustrated in Fig. 4.31, the geometry of the weld joint was separated into distinct portions based on the need.

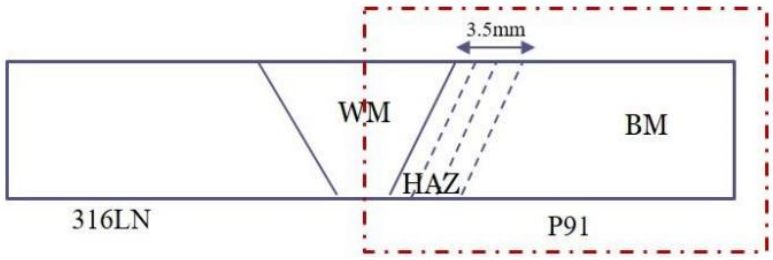

*WM: weld metal; BM; base metal; HAZ: heat affected zone

Fig. 4.4 P91 steel side of weldment for FE analysis

With consideration for the geometry of the weldment, a 2D mesh model was created. The table above was used to determine the necessary values for each component zone's creep coefficient, A, and strain exponent, n. The following von-Mises stress criteria were used as the basis for the FE analysis.

ISSN : 2583-6404
Nov - Dec 2023

$$\sigma_m = \sqrt{\frac{(\sigma_1 - \sigma_2)^2 + (\sigma_2 - \sigma_3)^2 + (\sigma_3 - \sigma_1)^2}{2}} \quad (4.3)$$

The maximum primary stress, denoted as σ1, represents the highest stress magnitude experienced in a given material. The intermediate stress, σ2, refers to the stress value that is between the maximum and minimum stresses. The minimum stress, σ3, represents the lowest stress magnitude encountered. Lastly, von-Mises' stress, denoted as σm, is a measure of the equivalent stress experienced in a material.

5. Conclusion

Regarding the size and distribution of M23C6 precipitates, there were the most significant microstructural changes. After PWHT, the microstructural alterations on the 316LN side were minimal. After welding, it was discovered that the P91 steel-weld interface had a straight fusion line whereas the 316LN stainless steel-weld interface had an epitaxial growth.

PWHT reduced the strength gradient on the P91 steel side in several areas. The IC-HAZ, which is the weakest zone of HAZ, had a remarkable recovery, as seen by the reduced mean KAM and LAGB proportion.

Reference

1. Cheepu, Muralimohan & Woo-SeongChe 2019, 'Characterization of microstructure and interface reactions in friction welded bimetallic joints of titanium to 304 stainless steel using nickel interlayer,'Transactions of the Indian Institute of Metals vol. 72, no.6, pp.1597-1601.
2. Hao, Xiaohu 2019, 'Microstructure and mechanical properties of laser welded TC4 titanium alloy/304 stainless steel joint with (CoCrFeNi) 100-xCux high-entropy alloy interlayer,' Journal of Alloys and Compounds vol. 803,pp. 649-657.
3. Scherillo & Fabio, 2019, 'Linear friction welding of Ti-6Al-4V parts produced by electron beam melting,' Materials and Manufacturing Processes vol. 34, no. 2, pp. 201-207.
4. Shen, Junqi 2017, 'Comparison of single-beam and dual-beam laser welding of Ti–22Al–25Nb/TA15 dissimilar titanium alloys,' Optics & Laser Technology vol. 93, pp. 118-126.
5. Sokolov, M 2015, 'Testing of new materials and computer aided optimization of laser beam welding of high-strength steels,' Physics Procediavol. 78, pp. 255-264.
6. Sordi&Vitor, L 2012, 'Microstructure and tensile strength of grade 2 titanium processed by equal-channel angular pressing and by rolling,' Journal of Materials Science vol. 47, no. 22, pp. 7870-7876.
7. Srinivas, B 2018, 'Studies on post weld heat treatment of dissimilar aluminum alloys by laser beam welding technique,' IOP ConfSer Mater Sci Eng. vol. 330,no. 012079.
8. Sun, Z 1996, 'Feasibility of producing ferritic/austenitic dissimilar metal joints by high energy density laser beam process,' International journal of pressure vessels and piping vol.68, no.2, pp. 153-160.
9. Sun, Zhe 2015, 'Investigation of droplet transfer behaviours in cold metal transfer (CMT) process on welding Ti-6Al-4V alloy,' The International Journal of Advanced Manufacturing Technology vol. 80, no.9-12,pp. 2007-2014.
10. Szwed, B & Konieczny, M2018, 'Structural changes during the formation of diffusion bonded joints between titanium and stainless steel,' IOP Conf. Ser. Mater. Sci. Eng. vol. 461.